Nanobody-Based RFP-Dependent Cre Recombinase for Selective Anterograde Tracing in RFP-Expressing Transgenic Animals

Ayumu Inutsuka (inutsuka@jichi.ac.jp)
Jichi Medical University https://orcid.org/0000-0001-6503-5501
Sho Maejima
Hiroyuki Mizoguchi
Ryosuke Kaneko
Rei Nomura
Keiko Takanami
Hirotaka Sakamoto
Okayama University https://orcid.org/0000-0002-6224-4591
Tatsushi Onaka
Jichi Medical University

Article

Keywords:

Posted Date: January 21st, 2022

DOI: https://doi.org/10.21203/rs.3.rs-1234462/v1

Version of Record: A version of this preprint was published at Communications Biology on September 16th, 2022. See the published version at https://doi.org/10.1038/s42003-022-03944-2.

Abstract

Transgenic animals expressing fluorescent proteins are widely used to label specific cells and proteins. GFP-dependent gene regulation utilizes these lines to manipulate gene expression; however, its application has been limited to fluorescent proteins derived from Aequorea jellyfish. By using a split Cre recombinase fused with mCherry-binding nanobodies or designed ankyrin repeat proteins, we created Cre recombinase dependent on red fluorescent protein (RFP) (Cre-DOR). Functional binding units for monomeric RFPs (mCherry, mRFP1) are different from those for dimeric RFP (tdTomato). We confirmed target RFP-dependent gene expression in the mouse cerebral cortex using stereotaxic injection of adeno-associated virus vectors including Cre-DOR, target RFP, and reporter GFP vector. We found highly selective GFP expression in RFP-positive cortical neurons with 93.5 ± 0.6% of GFP-positive cells being mRFP1-positive. In estrogen receptor-beta (*Esr2*)-mRFP1 mice, we confirmed that Cre-DOR can be used for selective expression of membrane-bound GFP in the paraventricular nucleus of the hypothalamus. The neural projection from Esr2-expressing neurons in the hypothalamic paraventricular nucleus to the posterior pituitary was visualized by Cre-DOR. In gastrin-releasing peptide receptor (*Grpr*)-mRFP1 rats, we similarly achieved anterograde tracing of Grpr-expressing neurons in the medial amygdala and found that they are projecting axons to the posterior bed nucleus of the stria terminalis. Cellular localization of RFPs affects recombination efficiency of Cre-DOR, and light and chemical-induced nuclear translocation of an RFP-fused protein can increase or decrease Cre-DOR efficiency. Our results provide a method for manipulating gene expression in specific cells expressing RFPs and expand the repertory of nanobody-based genetic tools.

Significance Statement

Genetically encoded fluorescent proteins are widely used to observe specific cells or proteins *in vivo*. We generated Cre recombinase dependent on RFP (Cre-DOR) by combining RFP-specific nanobodies with split-Cre. Cre-DOR can induce specific gene expression in mRFP1-positive neurons with 93.5 ± 0.6% specificity. Using this system in *Grpr*-mRFP1 transgenic rats, we found specific projection from the medial amygdala to the BNST. Translocation of target RFPs greatly affected the efficiency of Cre-DOR. Using the glucocorticoid receptor, we achieved chemical upregulation of Cre-DOR activity by inducing translocation of target RFPs from the cytosol to the nucleus. Our findings extend the potential use of RFP-expressing transgenic animals and provide a unique method to utilize nuclear translocation of signal molecules for genetic manipulation.

Introduction

To understand the precise roles of specific types of neurons, their visualization and manipulation in a living animal are required. Genetically encoded fluorescent proteins are widely used to identify and observe specific types of cells *in vivo*. There are various fluorescent proteins, but many of them are variants of green fluorescent proteins (GFPs) derived from Aequorea jellyfish (Chalfie et al., 1994; Nagai et al., 2002; Shaner et al., 2005) or red fluorescent proteins (RFPs) from Discosoma coral (Shaner et al.,

2004; Subach et al., 2009; Inoue et al., 2015). While the original coral RFP, DsRed, is obligately tetrameric (Baird et al., 2000), dimeric and monomeric variants have been created from DsRed (Campbell et al., 2002; Shaner et al., 2004). RFPs provide the inherent advantages of lower phototoxicity, lower autofluorescence, and deeper tissue penetration associated with longer wavelength excitation light (Shen et al., 2015). Therefore, various RFPs are used to visualize live cells in many transgenic RFP-expressing animals such as mice (Saederup et al., 2010; Fujihara et al., 2015), rats (Katoh et al., 2011; Uenoyama et al., 2015) and even larger animals (Chou et al., 2014; Yao et al., 2018). For selective manipulation of specific cells, driver lines expressing Cre recombinase are widely used. The combination of Cre driver mice and Cre-dependent virus vectors is an essential basis for optogenetics and chemogenetics in neuroscience. While recent genome-editing tools such as CRISPR-Cas systems have dramatically changed the generation of transgenic animals (Ran et al., 2013; Doudna and Charpentier, 2014; Heidenreich and Zhang, 2016), production and validation of a new Cre driver animal is still time-consuming, especially for large animals. Therefore, it would be useful if we could utilize existing well-characterized RFP-expressing animals to manipulate gene expression in specific cells by using Cre-dependent genetic tools.

Nanobodies are single-chain small antibodies derived from camels and they contain only one monomeric antigen-binding unit (Helma et al., 2015). Nanobodies and recombinant binders such as designed ankyrin repeat proteins (DARPins) (Binz et al., 2005; Stumpp et al., 2008) are frequently used as small molecular modules that selectively bind to target proteins. Specific recognition of target proteins by nanobodies can be utilized for not only visualization of target proteins (Irannejad et al., 2013; Yamagata and Sanes, 2018; Gerdes et al., 2020) but also protein degradation (Daniel et al., 2018), signal inhibition (Gulati et al., 2018) and property manipulation (Kirchhofer et al., 2010). Recently, GFP-dependent gene regulation methods using GFP-specific nanobodies have been reported (Tang et al., 2013; Tang et al., 2015). These techniques enable selective gene expression in GFP-expressing cells by utilizing nanobodies as specific binding modules to recognize GFPs. However, these methods have so far been limited to GFP variants and their applications to fluorescent protein-tagged endogenous proteins have not been fully studied.

In this study, we generated Cre recombinase dependent on RFPs (Cre-DOR) using nanobodies and DARPins. We found that functional binding unit pairs for monomeric RFPs (mCherry, mRFP1) are different from those for dimeric RFP (tdTomato). Using AAV vectors, we achieved highly selective expression of genes of interest *in vivo*. In *Est2-mRFP1* mice, we confirmed the utility of Cre-DOR for selective tracing of mRFP1-expressing neurons in mRFP1-expressing transgenic animals. In *Grpr*-mRFP1 rats, we achieved selective labeling of Grpr-expressing neurons in the medial amygdala and detected a specific neural pathway from the posterodorsal medial amygdala (MePD) to the posterior bed nucleus of the stria terminalis (BSTp). In addition, we found that the activity of Cre-DOR is affected by cellular localization of target RFPs, and we achieved optical and pharmacological control of Cre-DOR activity by utilizing nuclear translocation of target RFPs. Our results advance genetic manipulation tools using nanobodies and DARPins utilizing existing RFP-expressing transgenic animals even if useful Cre-driver lines do not exist.

Materials And Methods

Animals

All experimental procedures with mice were approved by the Institutional Animal Experiment Committee of Jichi Medical University. Male C57BL/6J mice were purchased from Charles River Laboratories Japan (Kanagawa, Japan). The mice were maintained under a 12-hour light/dark cycle (light period: 7:30-19:30, dark period: 19:30-7:30) in a room with controlled temperature (22 ± 2℃) and humidity (55 ± 15%). Food and water were available *ad libitum*. *Esr2*-mRFP1 transgenic mice were generated by Dr. Hirotaka Sakamoto and their validation was published (Sagoshi et al., 2020). *Grpr*-mRFP1 transgenic rats were also generated by Dr. Hirotaka Sakamoto and their validation was published (Takanami et al., 2021). Briefly, the *Grpr* promoter-human heparin-binding epidermal growth factor-like growth factor-2A-mRFP1 BAC transgene was purified for microinjection using a slight modification of the procedure described previously (Abe et al., 2004). *Grpr*-mRFP1 transgenic rats were generated by pronuclear injection of Wistar rat embryos (Institute of Immunology Co., Ltd., Tokyo, Japan). For experiments using *Esr2*-mRFP1 transgenic mice and *Grpr*-mRFP1 transgenic rats, adult transgenic animals bred in the animal facility of Okayama University were used. All of the *Grpr*-mRFP1 rats and *Esr2*-mRFP1 mice were maintained on a 12-h light/12-h dark cycle and were provided unlimited access to water and rodent chow. The Committee for Animal Research, Okayama University, Japan authorized the experimental procedures.

Drug administration and light illumination

Dexamethasone (Dex) was purchased from Merck (Darmstadt, Germany). Dex was dissolved in ethanol as a 1 mM stock solution and diluted with culture medium to 1 μM just after plasmid transfection. An LED flat panel light (TH2-100X100BL; CCS Inc., Kyoto, Japan) was used for uniform blue light illumination (465 nm, 3.7 W/m^2) of LEXY domains. The procedures for blue light stimulation were based on a previous report (Inutsuka et al., 2020). In Figure 3E and 3H, nuclei are visualized by fluorescence from Histone 2B-BFP (pAAV-EF1α-H2B-BFP-WPRE) that was co-transfected with mCherry-GR or nls-mCherry-LEXY.

DNA construction

Amino acid sequences of mCherry nanobodies (MBPs 1 - 6) were described in a previous report (Fridy et al., 2014) (originally described as LaMs 1 – 4, 6, and 8). DNA sequences of mCherry DARPins (MBP 7 and MBP 8) were described in another previous report (Brauchle et al., 2014) (originally described as 2m22 and 3m160). DNA sequences of MBPs 1 - 8 were codon-optimized, synthesized (Genscript, Piscataway, NJ), and inserted instead of GFP-specific nanobodies in pAAV-EF1α-N-CretrcintG (Addgene ID: 69570) or pAAV-EF1α-C-CreintG (Addgene ID: 69571) using NheI and EcoRI sites. Amino acid sequences of cellular localization signals were derived from previous reports (CAAX motif (Kawano et al., 2016), NES (Huang et al., 2013), and NLS (Beier et al., 2011)). GFP tagged with a palmitoylation signal (palGFP) has been used to efficiently trace neuronal fibers (Furuta et al., 2001). A vector coding palGFP was a kind gift from Dr.

Takahiro Furuta (Kyoto University). DNA sequences of Histone 2B (H2B), LEXY, glucocorticoid receptor (GR), and NanoLuc were derived from (Addgene ID: 2097), (Addgene ID: 72655), (NM_001364180.2) and pNL1.1 vector (Promega, Madison, WI, USA). They were synthesized with restriction enzyme sites and inserted into pAAV-EF1α-H2B-BFP-WPRE, pAAV-CAG-FLEX-H2B-GFP-WPRE, pAAV-EF1α-NLS-mCherry-LEXY-WPRE, pAAV-EF1α-mCherry-GR-WPRE, pAAV-EF1α-EGFP-GR-WPRE and pAAV-CAG-FLEX-NanoLuc-WPRE, respectively. The FLEX switch consists of paired loxP and lox2272 sequences and enables the expression of a gene of interest only when Cre recombinase is functional (Atasoy et al., 2008).

In vitro luciferase assay

Plasmids encoding EF1α-driven fluorescent target proteins and N- and C-terminal split Cre chimeric variants were transfected by calcium phosphate into HEK293 cells (AAV293 cells purchased from Agilent Technologies, Inc., Santa Clara, CA, USA) along with plasmids encoding pAAV-CAG-FLEX-NanoLuc. Between 100 and 200 ng of total DNA was transfected into single wells of 96-well plates. Cells were ~80–100% confluent at the time of transfection. Cells were harvested one day (Figures 1 and 3) or two days (Figure 3F) later for the Nano-Glo Luciferase Assay System (Promega). All transfections were done at equal plasmid molar ratios. We used a Spark10M multimode microplate reader (TECAN, Männedorf, Switzerland) to detect luminescence.

Adeno-associated virus (AAV) production and purification

All AAV vectors were produced using the AAV Helper-Free System (Agilent Technologies, Inc., Santa Clara, CA, USA) and purified on the basis of published methods (Inutsuka et al., 2016). Briefly, HEK293 cells were transfected with a pAAV vector plasmid that included a gene of interest, pHelper and pAAV-RC (serotype 9; purchased from Penn Vector Core, Philadelphia, PA, USA) using the standard calcium phosphate method. Three days later, transfected cells were collected and suspended in artificial cerebrospinal fluid (aCSF; 124 mM NaCl, 3 mM KCl, 26 mM $NaHCO_3$, 2 mM $CaCl_2$, 1 mM $MgSO_4$, 1.25 mM KH_2PO_4, and 10 mM D-Glucose). After 4 freeze-thaw cycles, the cell lysate was treated with benzonase nuclease (Merck, Darmstadt, Germany) at 45°C for 15 min and centrifuged 2 times at 16,000 g for 10 min. The supernatant was used as the virus-containing solution. To measure the titer of purified virus, the supernatant was dissolved in artificial CSF. Digital PCR was performed to measure the viral titer using TaqMan MGB probes and the following primer pairs: woodchuck hepatitis virus posttranscriptional regulatory element (WPRE): 5'-VIC-CTGCTTTAATGCCTTTGTAT-MGB-3', Forward: 5'-TGCTCCTTTTACGCTATGTGGATA-3', Reverse: 5'-CATAAAGAGACAGCAACCAGGATTT-3'; human growth hormone polyA: 5'-FAM-CACAATCTTGGCTCACTG-MGB-3', Forward: 5'-GGGTCTATTGGGAACCAAGCT-3', Reverse: 5'-GGCTGAGGCAGGAGAATCG-3'. The AAV vector was stored at -80°C in small aliquots until the day of the experiment.

Stereotaxic AAV injection

Surgeries for AAV injections were conducted using a stereotaxic instrument. In Cre-DOR C57BL/6J mouse experiments (Figure 4), 600 nl of a mixture of AAV9-EF1α-NCre-MBP6-WPRE (1 x 10^{12} vg/ml), AAV9-EF1α-

CCre-MBP1-WPRE (1 x 10^{12} vg/ml), AAV9-CAG-FLEX-nlsGFP-WPRE (1 x 10^{12} vg/ml), and AAV9-EF1α-mRFP1-WPRE (5 x 10^{10} vg/ml) or AAV9-EF1α-mRuby-WPRE (5 x 10^{10} vg/ml) was injected in the right hemisphere M1 cortex (from bregma +0.7 mm, lateral +1.7 mm, ventral -0.8 mm) of 10-week-old male C57BL/6J mice. In *Esr2*-mRFP1 mouse experiments (Figure 5), 1 µl of a mixture of AAV9-EF1α-NCre-MBP6-WPRE (final concentration in the mixture: 6 x 10^{12} vg/ml), AAV9-EF1α-CCre-MBP1-WPRE (6 x 10^{12} vg/ml) and AAV9-CAG-FLEX-palGFP-WPRE (6 x 10^{12} vg/ml) was injected in the paraventricular nucleus of the hypothalamus (PVN) (from bregma -0.9 mm, lateral 0.2 mm, ventral -4.3 mm) of 12-14-week-old male and female *Esr2*-mRFP1 transgenic or control wild-type mice. In *Grpr*-mRFP1 rat experiments (Figure 6), 1 µl of a mixture of AAV9-EF1α-NCre-MBP6-WPRE (final concentration in the mixture: 6 x 10^{12} vg/ml), AAV9-EF1α-CCre-MBP1-WPRE (6 x 10^{12} vg/ml) and AAV9-CAG-FLEX-palGFP-WPRE (6 x 10^{12} vg/ml) was injected in the medial amygdala area (from bregma -3.0 mm, lateral ±3.5 mm, ventral -9.0 mm) of 10–15-week-old female *Grpr*-mRFP1 transgenic or control wild-type rats. Rat brain atlas figures were derived from Swanson, L.W. (2004) Brain maps: structure of the rat brain, 3rd edition (Creative Commons Attribution-NonCommercial 4.0 International License).

Retrograde tracing using retrobeads

Surgeries for injections of retrobeads were conducted using a stereotaxic instrument. In *Grpr*-mRFP1 rat experiments (Figure 5), 300 nl of Green Retrobeads™ IX (Lumafluor, Durham, NC) was injected in the BSTp (from bregma -1.1 mm, lateral 0.8 mm, ventral -7.4 mm) of 9 - 10-week-old female *Grpr*-mRFP1 transgenic rats. The rats were perfused one week after injection.

Immunohistochemistry and fluorescence microscopy

Three to four weeks after virus injections, mice were deeply anesthetized by Avertin and transcardially perfused with heparinized saline (20 U/ml) followed by 4% paraformaldehyde in 0.1 M phosphate buffer (pH, 7.4). Brains were removed, post-fixed in 4% paraformaldehyde solution overnight, and transferred to 30% sucrose solution in 0.1 M phosphate buffer until they sank. Series of 40-µm-thick (Figure 4) or 30-µm-thick (Figures 5 and 6) sections were obtained with a cryostat (CryoStar NX70; Thermo Fisher Scientific, Waltham, MA, USA). For staining, coronal brain sections were immersed in a blocking buffer (10% goat serum and 0.3% Triton-X in 0.1 M PBS) and then incubated with primary antibodies at 4°C overnight. The sections were washed with the blocking buffer and then incubated with secondary antibodies for 1 hour at RT. The brain sections were mounted and examined with a fluorescence microscope (IX73, Olympus, Tokyo, Japan). Primary antibodies and secondary antibodies were diluted in the blocking buffer as follows: anti-GFP (RRID: AB591816, Medical & Biological Laboratories, Tokyo, Japan) at 1:1000 and Alexa Fluor 488 goat anti-rabbit IgG (diluted 1:1000; 1-day incubation at 4°C; A11034; Thermo Fisher Scientific). For the images shown in Figures 5 and 6, we used anti-GFP (RRID: AB1537403, Rockland Immunochemicals, Limerick, PA) at 1:2000, rabbit anti-DsRed (RRID: AB10013483, Takara Bio, Japan) at 1: 1000, Alexa Fluor 488 goat anti-chicken IgY (diluted 1:1000; 103-545-155; Jackson ImmunoResearch Laboratories, West Grove, PA) and Alexa Fluor 546 goat anti-rabbit IgG (diluted 1:1000; 111-546-003; Jackson ImmunoResearch Laboratories). We manually counted fluorescence-

positive cells using NIH ImageJ software and calculated the relative percentage of fluorescence-positive cells. For counting in Figure 4, we analyzed one out of every four coronal brain slices.

Statistical Analysis

Statistical analyses were performed using GraphPad Prism 9 for Windows (GraphPad Software, San Diego, CA). Simple comparisons of the means and SEM were performed by Student's t-test. Multiple comparisons of the means and SEM were performed by one-way ANOVA followed by Tukey's test. A P value of less than 0.05 was considered significant in these analyses.

Results

Screening of efficient mCherry-binding protein (MBP) pairs to design Cre recombinase dependent on RFPs

First, we aimed to construct Cre recombinase dependent on RFPs based on the reported tool named Cre-DOG (Tang et al., 2015). In this system, N-terminal and C-terminal split Cre recombinase fragments are fused with specific nanobodies for target proteins, and target proteins mediate reunion of the split Cre recombinase fragments (Figure 1A). In order to identify functional pairs of binding proteins, we selected 6 nanobodies and 2 DARPins previously reported to have a highly specific binding property to a monomeric RFP, mCherry (Brauchle et al., 2014; Fridy et al., 2014), and we constructed every combination (8 + 8 = 16 constructs). The codon-optimized DNA sequences were synthesized and were inserted instead of GFP-specific nanobodies in pAAV-EF1α-N-CretrcintG (Addgene ID: 69570) or pAAV-EF1α-C-CreintG (Addgene ID: 69571) using NheI and EcoRI sites. We renamed them as MBPs (mCherry-binding proteins) 1 – 8 in this study. MBPs 1-6 are nanobodies and MBPs 7 and 8 are DARPins. As a consequence, we obtained pAAV-EF1α-N-Cre-MBP(1-8)-WPRE and pAAV-EF1α-C-Cre-MBP(1-8)-WPRE.

Then we performed *in vitro* luciferase reporter assays to find adequate MBP pairs that could induce reunion to reconstruct an active Cre recombinase. N-Cre-MBP, C-Cre-MBP, FLEX-NanoLuc, and target RFPs were co-transfected into HEK293 cells by the calcium phosphate method. The FLEX switch consists of paired loxP and lox2272 sequences and enables the expression of a gene of interest only when Cre recombinase is functional (Atasoy et al., 2008). NanoLuc is a small and bright luciferase from the deep-sea shrimp *Oplophorus gracilirostris* (Hall et al., 2012). Recombinase activities were measured as luminescence derived from the bioluminescent reaction catalyzed by NanoLuc luciferase. We tested mCherry, mRFP1, and tdTomato as target proteins. These red fluorescent proteins were all derived from the same wild-type DsRed protein (Shaner et al., 2004). While mCherry and mRFP1 are monomeric, tdTomato is a tandem dimer of two subunits. We also tested mRuby, which is a monomeric variant of the red fluorescent protein eqFP611 derived from *Entacmaea quadricolor* (Kredel et al., 2009), as a negative control. As shown in Figure 1B and 1C, heat maps of mCherry and mRFP1 showed similar patterns. The pair of N-Cre-MBP6 and C-Cre-MBP1 induced high activity for both mCherry and mRFP1. Twin pairs of the same MBP such as N-Cre-MBP1 and C-Cre-MBP1 or N-Cre-MBP2 and C-Cre-MBP2 showed weak reporter

activities, possibly indicating competition for the same binding site by both N-Cre-MBP and C-Cre-MBP. On the other hand, the heat map for tdTomato greatly differed from those of mCherry and mRFP1 (Figure 1D). Unfortunately, we did not find any strong signal when we targeted the tetrameric RFP, DsRed (Figure 1E). The twin pair of N-Cre-MBP8 and C-Cre-MBP8 showed the highest activity for tdTomato. The heat maps for mRuby and No RFPs (Figure 1F and 1G) showed only weak recombinase activities around the maps. According to these heat maps obtained from luciferase assays, we selected the pair of N-Cre-MBP6 and C-Cre-MBP1 as a candidate pair for Cre-dependent on monomeric RFP.

Characterization of recombinase activity of Cre-DORs in vitro

Next, we investigated the recombination efficiency of the pair of N-Cre-MBP6 and C-Cre-MBP1 (Cre-DOR^{N6C1}) using a fluorescent protein reporter. Four kinds of plasmids including N-Cre-MBP6, C-Cre-MBP1, target RFPs, and FLEX-H2B-GFP were co-transfected into HEK293 cells by the calcium phosphate method (Figure 2A). H2B-GFP shows nuclear localization because H2B (histone 2B) protein binds to the DNA in the nucleus. Recombinase activities were measured as H2B-GFP expression induced by FLEX switching (Figure 2B). The fluorescent signal of GFP was enhanced by immunostaining using a GFP antibody. Quantitative cell counting of fluorescent images showed that 81.8 ± 1.5% of mCherry-positive cells were GFP-positive and that 74.1 ± 1.6% of mRFP1-positive cells were GFP-positive, while 5.6 ± 0.6% of mRuby-positive cells were GFP-positive (n = 8 each) (Figure 2C, 2D). The recombination efficiency of Cre-DOR^{N6C1} + mCherry was 14.6-times higher than that of Cre-DOR^{N6C1} + mRuby. The Cre-DOR^{N6C1} system was found to be dependent on all three components of target RFPs, N-Cre-MBP6, and C-Cre-MBP1 in the system. Removal of N-Cre-MBP6 or C-Cre-MBP1 resulted in total loss of reporter activity. Cell counting showed that 0.9 ± 0.1% of mRFP1-positive cells were GFP-positive without CCre-MBP1 and that 0.8 ± 0.1% of mRFP1-positive cells were GFP-positive without NCre-MBP8 (n = 8 each). In all cases, the percentages of RFP-positive cells in GFP-positive cells were higher than 90% possibly because of the transfection method (mCherry: 98.9 ± 0.3%, mRFP1: 98.3 ± 0.3%, mRuby: 91.0 ± 1.9%, mRFP1ΔCCre: 94.4 ± 3.7%, mRFP1ΔNCre: 88.5 ± 5.6%).

We also tested the recombination efficiency of the pair of N-Cre-MBP5 and C-Cre-MBP4 (Cre-DOR^{N5C4}). Quantitative cell counting of fluorescent images showed that 57.9 ± 1.6% of mCherry-positive cells were GFP-positive and that 9.3 ± 1.1% of mRFP1-positive cells were GFP-positive, while only 0.9 ± 0.1% of mRuby-positive cells were GFP-positive (n = 8 each) (Figure 2E, 2F). The recombination efficiency of Cre-DOR^{N5C4} + mCherry was 61.0 times-higher than that of Cre-DOR^{N5C4} + mRuby. The Cre-DOR^{N5C4} system was also found to be dependent on all three components of target RFPs, N-Cre-MBP5, and C-Cre-MBP4 in the system. Removal of N-Cre-MBP5 or C-Cre-MBP4 resulted in total loss of reporter activity. Cell counting showed that 0.7 ± 0.1% of mRFP1-positive cells were GFP-positive without CCre-MBP4 and that 0.8 ± 0.2% of mRFP1-positive cells were GFP-positive without NCre-MBP5 (n = 8 each). Although Cre-DOR^{N5C4} can induce more specific recombination dependent on mCherry, we decided to use Cre-DOR^{N6C1} in the later *in vivo* experiments because of its high efficiency when it was applied for mRFP1.

In the heatmap of the luciferase assay shown in Figure 1D, we found that the pair of N-Cre-MBP8 and C-Cre-MBP8 shows the highest recombination efficiency dependent on tdTomato. Therefore, we also tested the recombination efficiency of the pair of N-Cre-MBP8 and C-Cre-MBP8 (Cre-DOR^{N8C8}). Quantitative cell counting of fluorescent images showed that 46.9 ± 1.1% of tdtomato-positive cells were GFP-positive, while 12.8 ± 1.2% of mRuby-positive cells were GFP-positive (n = 4 each) (Figure 2G). Although Cre-DOR^{N8C8} shows mild specificity against tdTomato, we thought that the S/N ratio of Cre-DOR^{N8C8} was not sufficiently high for use *in vivo*.

Cellular Localization Of Target Rfps Affects Cre-dor Activity

Cre recombinase exerts its activity within the nucleus. Therefore, it is possible that cellular localization of target RFPs affects Cre-DOR recombinase activity. In order to test this hypothesis, we created mCherry and tdTomato fused with various localization signal peptides: CAAX motif for membrane localization, NES for cytosolic localization, and NLS for nuclear localization (Figure 3A). We observed clear intracellular translocalization of mRFP1 and tdTomato by being fused with these motifs. mCherry/tdTomato fused with CAAX were localized in the plasma membrane, mCherry/tdTomato fused with NES were localized in the cytosol, mCherry/tdTomato without any motif were localized in both the cytosol and nucleus, and nls-mCherry/tdTomato were localized in the nucleus (Figure 3B). Next, we performed *in vitro* luciferase reporter assays to investigate the effect of cellular translocation on recombinase activity. Plasmids for N-Cre-MBP, C-Cre-MBP, FLEX-NanoLuc, and target RFPs were co-transfected into HEK293 cells. When Cre-DOR^{N6C1} or Cre-DOR^{N8C8} targets RFPs with localization signals, the luciferase assay showed a clear difference between the cellular localizations (Figure 3C). A gradual incremental tendency of recombination activity among membrane-bound, cytosolic, and nucleic localization of target RFPs was observed. Quantitative analyses of luciferase assay data showed that recombinase activity is significantly different between Cre-DOR^{N6C1}/Cre-DOR^{N8C8} + mCherry/tdTomato-NES and Cre-DOR^{N6C1}/Cre-DOR^{N8C8} + nls-mCherry/tdTomato ($P < 0.0001$, Tukey's multiple comparison test, n = 11). Note that average fluorescence intensity of mCherry-NES or tdTomato-NES is higher than that of nls-mCherry or nls-tdTomato.

Next, we aimed to control Cre-DOR activity by using chemical ligands. Glucocorticoid receptor (GR) is a nuclear receptor and it is translocated into the nucleus after binding its ligand, glucocorticoid (Lupien et al., 2009) (Figure 3D). Ligand-induced translocation of GR has been detected by addition of a GFP to the N-terminus of GR (Htun et al., 1996; Mikuni et al., 2007). Therefore, we attached RFPs to human glucocorticoid receptor alpha (hGRα) in order to control Cre-DOR activity. We found that mCherry-GR was localized in the cytosol without its ligand, dexamethasone (Dex) and that it translocated to the nucleus after incubation with Dex (1 μM, 1 hour) (Figure 3E). In Figure 3E, nuclei are visualized by fluorescence from Histone 2B-BFP (pAAV-EF1α-H2B-BFP-WPRE) that was co-transfected with mCherry-GR. Cre recombinase activity of Cre-DOR^{N6C1} targeting mCherry-GR was strongly increased by the presence of Dex (Figure 3F).

An increase in Cre recombinase activity by nuclear localization of RFPs suggests that Cre-DOR activity can be manipulated by controlling the intracellular localization of target RFPs. In order to test this hypothesis, we used a light-inducible nuclear export domain called LEXY (Niopek et al., 2016). LEXY consists of an engineered LOV2 domain from *Avena sativa* phototropin-1 (AsLOV2), in which the C-terminal Jα helix was converted into an artificial NES. In the dark, the NES is tightly packed against the AsLOV2 core and is thus inactive. Exposure to blue light induces unfolding of the modified Jα helix, uncovering the NES (Figure 3G). We confirmed that nls-mCherry-LEXY was localized mainly in the nucleus in the dark, and blue light illumination (465 nm, 7 W/m^2) induced translocation of fused RFPs into the cytosol in 30 min (Figure 3H). In Figure 3H, nuclei are visualized by fluorescence from Histone 2B-BFP that was co-transfected with nls-mCherry-LEXY. We found that blue light illumination inhibited Cre recombination activity of Cre-DOR^{N6C1} targeting nls-mCherry-LEXY as indexed by luciferase activity (Figure 3I).

Functional assay of Cre-DOR in vivo **using AAV vectors**

In order to examine whether Cre-DOR^{N6C1} functions in living animals, we generated AAV vectors encoding N-Cre-MBP6, C-Cre-MBP1, FLEX-nlsGFP, and target RFPs. GFP tagged with a nuclear localization signal (nlsGFP) is localized mainly in the nucleus. 600 nl of a mixture of virus vectors for Cre-DOR^{N6C1}, FLEX-nlsGFP (1 x 10^{12} vg/ml each), and target mRFP1 (5 x 10^{10} vg/ml) was unilaterally injected into the right side M1 cortex of wild-type 10-week-old male mice (Figure 4A). The titer of the target RFP-expressing vector was lowered to induce scattered expression and make it easy to count fluorescent protein-expressing cells separately. Recombinase activities were measured as nlsGFP expression induced by FLEX switching (Figure 4B). Four weeks after injection, mice were sacrificed for immunohistochemistry and brain slices were stained with anti-GFP. Clear expression of nlsGFP at the injected site in the M1 cortex was observed (Figure 4C). Quantitative cell counting of fluorescent images showed that 50.2 ± 2.5% of mRFP1-positive cells were GFP-positive and that 93.5 ± 0.6% of GFP-positive cells were mRFP1-positive (n = 5 each) (Figure 4D, 4E). The expression efficiency of GFP in the center area of injection was higher than that in the peripheral area. In order to check the specificity of the Cre-DOR^{N6C1} system *in vivo*, we injected vectors for Cre-DOR^{N6C1}, FLEX-nlsGFP (1 x 10^{12} vg/ml each), and mRuby (5 x 10^{10} vg/ml) as a control (Figure 4F). While we observed comparative amounts of mRuby-expressing neurons in the M1 cortex, we found only sparce nlsGFP-expressing neurons in the same area (Figure 4G). Quantitative cell counting of nlsGFP and mRuby-positive cells showed a clear difference between Cre-DOR^{N6C1} + mRFP1-injected mice and Cre-DOR^{N6C1} + mRuby-injected mice. The cell counting showed that 1.5 ± 0.5% of mRuby-positive cells were GFP-positive and that 13.3 ± 4.1% of GFP-positive cells were mRuby-positive (n = 5 each) (Figure 4D, 4E). The recombination efficiency of Cre-DOR^{N6C1} + mRFP1 was 34.4-times higher than that of Cre-DOR^{N6C1} + mRuby in these experiments. All these data suggest *in vivo* specificity of the Cre-DOR^{N6C1} system using AAV vectors.

Functional Assay Of Cre-dor In Mrfp1-expressing Transgenic Mice

Next, we examined selective expression by Cre-DOR^{N6C1} in mRFP1-expressing transgenic animals. In *Esr2*-mRFP1 mice, neurons in the paraventricular nucleus (PVN) are visualized by mRFP1. 1 µl of a mixture of AAV9-EF1α-NCre-MBP6-WPRE (6 x 10^{12} vg/ml), AAV9-EF1α-CCre-MBP1-WPRE (6 x 10^{12} vg/ml) and AAV9-CAG-FLEX-palGFP-WPRE (6 x 10^{12} vg/ml) was injected in the PVN of *Esr2*-mRFP1 transgenic mice (Figure 5A). Recombinase activities were measured as expression of GFP tagged with a palmitoylation signal (palGFP) induced by FLEX switching (Figure 5B). palGFP is sorted to the plasma membrane and has been used to trace neuronal fibers anterogradely (Furuta et al., 2001; Nasanbuyan et al., 2018). Four weeks after injection, mice were sacrificed for immunohistochemistry and brain slices were stained with anti-GFP and anti-mRFP1. Clear expression of palGFP at the injected site in the PVN was observed (Figure 5C). It has been reported that mRFP1-expressing neurons in the PVN of *Esr2*-mRFP1 mice include oxytocin neurons (Sagoshi et al., 2020) and oxytocin neurons send their axons into the posterior pituitary. In accordance with these previous findings, we observed clear projection from the palGFP-expressing neurons in the PVN and dense axonal terminals in the posterior pituitary (Figure 5D). Quantitative cell counting of palGFP-positive cells in the PVN showed a clear difference between mRFP(+) mice and mRFP(-) mice (Figure 5E). The cell counting showed that 24.1% of mRFP1-positive neurons in the PVN express palGFP on average (Figure 5F). These results showed the usability of Cre-DOR^{N6C1} for detection of selective neural projection in mRFP1-expressing transgenic animals. We also confirmed that Cre-DOR^{N6C1} can be functional in other parts of the brain such as the islands of Calleja (ICj) in *Esr2*-mRFP1 mice **(Supplemental Figure 1)**.

Anterograde tracing of mRFP1-expressing neurons in Grpr-mRFP1 rats

Finally, we examined selective expression by Cre-DOR^{N6C1} in mRFP1-expressing transgenic animals. In gastrin-releasing peptide receptor (*Grpr*)-mRFP1 transgenic rats, neurons in the posterior amygdala are visualized by mRFP1. 1 µl of a mixture of AAV9-EF1α-NCre-MBP6-WPRE (6 x 10^{12} vg/ml), AAV9-EF1α-CCre-MBP1-WPRE (6 x 10^{12} vg/ml) and AAV9-CAG-FLEX-palGFP-WPRE (6 x 10^{12} vg/ml) was injected in the medial amygdala area of male *Grpr*-mRFP1 transgenic rats (Figure 6A). Four weeks after injection, rats were sacrificed for immunohistochemistry and brain slices were stained with anti-GFP and anti-mRFP1. Clear and selective expression of palGFP at the injected site in the posterodorsal medial amygdala (MePD) was observed (Figure 6B). We observed clear projection from the palGFP-expressing neurons in the MePD. We found a bundle of smooth passing fibers in the stria terminalis (ste) and dense axonal terminals with varicosity in the posterior bed nucleus of the stria terminalis (BSTp or STMP) (Figure 6C). These findings suggest that mRFP-expressing neurons in the MePD send their axons to the BSTp (Figure 6E). Finally, we confirmed this neural projection using a retrograde tracer. We injected 300 nl of green retrobeads in the BSTp of *Grpr*-mRFP1 transgenic rats (Figure 6D). One week after injection, rats were sacrificed. We detected some mRFP1 neurons that included green retrobeads in the MePD. These

results support our idea that mRFP-expressing neurons in the MePD send their axons to the BSTp (Figure 6F).

Discussion

In this study, we generated Cre recombinase dependent on RFPs (Cre-DOR) by making use of split-Cre combined with nanobodies and DARPins as binding units for target RFPs (Figure1). Cre recombinase activity was selectively induced by a monomeric RFP or by a dimeric RFP *in vitro* (Figure 2). The efficiency of Cre-DOR is affected by intracellular localization of target RFPs, and we achieved optical and pharmacological manipulation of Cre-DOR activity by utilizing intracellular translocation of the LINuS and glucocorticoid receptor (Figures 3). Using AAV vectors, we confirmed the efficiency and fidelity of selective induction of Cre-DOR activity in the mouse brain (Figures 4). Cre-DOR induced mRFP1-dependent expression of palGFP in *Esr2*-mRFP1 transgenic mice (Figures 5). We also achieved anterograde tracing of RFP-expressing neurons using Cre-DOR and found neural projection from mRFP-expressing neurons in the MePD to the BSTp in *Grpr*-mRFP1 transgenic rats (Figures 6).

Our results provide a new method for utilizing existing RFP transgenic animal lines to regulate gene expression selectively in RFP-expressing cells. This technique is useful not only because it can be used as a substitute of Cre transgenic lines but also because it can fundamentally provide a unique way to mark RFP-expressing cells. The number of available transgenic large animals including non-human primates has been gradually increasing (Sasaki et al., 2009; Liu et al., 2016; Yao et al., 2018). Although genome editing and other genetic techniques are being rapidly developed, it is still time-consuming to generate new transgenic animals, especially large animals. In addition, it is common to use 2A peptide for simultaneous expression of both Cre recombinase and fluorescent proteins in transgenic animals (Inutsuka et al., 2014; Hernandez et al., 2015). However, a tandem sequence linked with 2A peptide can induce unpredictable cis regulation of expression in some cases (Wang et al., 2021). Therefore, this simultaneous expression of Cre recombinase and fluorescent proteins using 2A peptide is not complete substitute for RFP-transgenic animals. Our method provides an efficient way to use the same transgenic line for different purposes.

Our findings using Cre-DOR provide valuable information on specific neural pathways in mRFP1-expressing transgenic animals. In *Esr2*-mRFP1 transgenic mice, we found that estrogen receptor β-expressing neurons in the PVN send their axons in the posterior pituitary (Figures 5D). We also reported that 70–80% of oxytocin neurons expressed mRFP1, while only 10% of vasopressin neurons did so in the PVN of *Esr2*-mRFP1 transgenic mice (Sagoshi et al., 2020). Estrogen has been found to both reduce anxiety-related behaviors and increase oxytocin peptide transcription, suggesting a role for oxytocin in this estrogen receptor β-mediated anxiolytic effect (Acevedo-Rodriguez et al., 2015). Considering that estrogen receptor α is not expressed in oxytocin neurons (Suzuki and Handa, 2005), it is reasonable to assume that estrogen receptor β in oxytocin neurons in the PVN plays a main role in this modulation. The absence of good antibodies for immunostaining for estrogen receptor β and the nuclear localization of estrogen receptor β hinder selective neural tracing of estrogen receptor β-expressing neurons in the PVN

so far. Our findings provide a good way to investigate the physiological role of this specific neural pathway.

In *Grpr*-mRFP1 transgenic rats, we found that Grpr-expressing neurons in the MePD send their axons to the BSTp (Figures 6C). Grpr neurons play an important role in emotional responses, social interaction, and feeding behavior (Roesler and Schwartsmann, 2012). Although Grpr neurons in the lateral amygdala are frequently investigated, Grpr neurons in the medial amygdala are not well studied so far. It has been reported that the anterior and posterior medial amygdala differentially innervate downstream targets. While the anterior medial amygdala densely innervates the horizontal diagonal band of Broca and the medial olfactory tubercle, the posterior medial amygdala innervates the BNST (DiBenedictis et al., 2014). Our findings using Cre-DOR support these previous anatomical works and suggest a functional linkage between Grpr and sexual behaviors.

We generated monomeric/dimeric state-specific RFP-dependent Cre (Figure 2). Functional properties of MBP pairs seem to reflect the difference of oligomerization states among mCherry, mRFP1, tdTomato, and DsRed. Theoretically, it is reasonable to assume that pairs of identical MBPs do not work for monomeric RFPs because of binding competition on a single recognition site. Indeed, we found low luciferase activity when we used mCherry or mRFP1 as a target protein for pairs of identical MBPs (Figure 1B, 1C). However, we found that the combination of N-Cre-MBP8 and C-Cre-MBP8 is a functional pair for tdTomato. These findings show that it can be essential to prepare multiple nanobodies for designing nanobody-dependent molecular tools, while it is possible to make a Cre-DOR-like system using only one nanobody if the target proteins form homodimers within the cell. Since tdTomato is a dimeric protein, the same recognition site should be exposed at two locations in one dimer. The functional property of Cre-DOR^{N8C8} might be utilized to detect the oligomerization state of monomeric proteins. For example, photo-induced conversion of the oligomerization state of a fluorescent protein, Dronpa, was reported (Zhou et al., 2012). Since Dronpa is also derived from its original coral tetramer protein (Ando et al., 2004), it is reasonable to establish a similar system using mCherry. Light-induced dimerization of small proteins has been reported (Imayoshi et al., 2013; Kawano et al., 2015). These systems would make it possible to achieve photo-induced switching of Cre recombinase activity.

We revealed that the Cre-DOR system is dependent on nuclear localization of target RFP proteins (Figure 3). Our findings show a limitation of Cre-DOR application *in vivo*. It might be difficult to use our Cre-DOR system for selective gene expression in cells expressing membrane protein fused with RFPs such as channelrhodopsin 2-mCherry or hM3Dq-mCherry in transgenic animals. On the other hand, our findings suggest that the Cre-DOR system can be used for clarification of nuclear translocation of proteins such as nuclear receptors. Cre-DORs showed minimal activity for cell membrane-localized target RFPs and high activity for nucleus-localized RFPs (Figure 3C). Therefore, it might be a good way to target membrane proteins that change their localization from the plasma membrane to the nucleus. In Notch signaling, the intercellular domain of Notch (NICD), which is a single-pass transmembrane receptor protein, is cleaved and translocates into the nucleus (Kopan and Ilagan, 2009). Amyloid beta is derived from amyloid precursor protein (APP) cleavage by γ-Secretase. Another cleavage fragment, APP

intracellular domain (AICD), is also known to translocate into the nucleus, inducing the expression of related genes (Gertsik et al., 2014). With specific binding proteins, these molecules can be targeted by a similar method for specific gene manipulation of signal-on cells in the future.

In the future, it will be possible for endogenous proteins to be used as targets for split-Cre systems. Our results showed that not only nanobodies but also DARPins can be used to construct functional molecules utilizing selective binding to target proteins for reunion of split-Cre. Therefore, when multiple specific nanobodies or other binding proteins exist, it might be possible to induce selective gene expression dependent on a target endogenous protein. Indeed, we can easily find multiple promising nanobodies for endogenous proteins in an open website database (Wilton et al., 2018). In addition, a rapid approach to generate large repertoires of recombinant nanobodies and *de novo* proteins designed for creating customized small binding proteins have been reported (Fridy et al., 2014; Chevalier et al., 2017). GFP-dependent Flp recombinase has also been reported (Tang et al., 2016). It will be useful to employ Cre-DOR with GFP-dependent Flp recombinase at the same time to manipulate two kinds of cells in the same animal **(Supplemental Figure 2)**.

Declarations

Acknowledgements: This work was supported by KAKENHI grants (16K08527, 16H01488, 17H06061 to A.I.; 17H04026, 17K19636, 25118008 to T.O.). A.I. was also supported by Jichi Medical University Young Investigator Award and a grant from Japan Prize Foundation. We thank Ms. Junko Kato for technical assistance. We thank Dr. T. Furuta (Kyoto University) for the generous gift of a vector coding palGFP. This work was also supported by the program for Brain Mapping by Integrated Neurotechnologies for Disease Studies (Brain/MINDS) from Japan Agency for Medical Research and Development, AMED, under the grant number JP19dm0207057.

Author Contributions

A.I. and T.O. designed the experiments; A.I., S. M., H.M., R.K., R.N., K.T., and H.S. performed the experiments; A.I., S. M., H.M., R.K., R.N., K.T., and H.S. contributed to the analysis and interpretation of data; A.I. and T.O. wrote the manuscript.

References

1. Abe K, Hazama M, Katoh H, Yamamura K, Suzuki M (2004) Establishment of an efficient BAC transgenesis protocol and its application to functional characterization of the mouse Brachyury locus. Exp Anim 53:311-320.
2. Acevedo-Rodriguez A, Mani SK, Handa RJ (2015) Oxytocin and Estrogen Receptor beta in the Brain: An Overview. Front Endocrinol (Lausanne) 6:160.
3. Ando R, Mizuno H, Miyawaki A (2004) Regulated fast nucleocytoplasmic shuttling observed by reversible protein highlighting. Science 306:1370-1373.

4. Atasoy D, Aponte Y, Su HH, Sternson SM (2008) A FLEX switch targets Channelrhodopsin-2 to multiple cell types for imaging and long-range circuit mapping. J Neurosci 28:7025-7030.
5. Baird GS, Zacharias DA, Tsien RY (2000) Biochemistry, mutagenesis, and oligomerization of DsRed, a red fluorescent protein from coral. Proc Natl Acad Sci U S A 97:11984-11989.
6. Beier KT, Samson ME, Matsuda T, Cepko CL (2011) Conditional expression of the TVA receptor allows clonal analysis of descendents from Cre-expressing progenitor cells. Dev Biol 353:309-320.
7. Binz HK, Amstutz P, Pluckthun A (2005) Engineering novel binding proteins from nonimmunoglobulin domains. Nat Biotechnol 23:1257-1268.
8. Brauchle M, Hansen S, Caussinus E, Lenard A, Ochoa-Espinosa A, Scholz O, Sprecher SG, Pluckthun A, Affolter M (2014) Protein interference applications in cellular and developmental biology using DARPins that recognize GFP and mCherry. Biol Open 3:1252-1261.
9. Campbell RE, Tour O, Palmer AE, Steinbach PA, Baird GS, Zacharias DA, Tsien RY (2002) A monomeric red fluorescent protein. Proc Natl Acad Sci U S A 99:7877-7882.
10. Chalfie M, Tu Y, Euskirchen G, Ward WW, Prasher DC (1994) Green fluorescent protein as a marker for gene expression. Science 263:802-805.
11. Chevalier A et al. (2017) Massively parallel de novo protein design for targeted therapeutics. Nature 550:74-79.
12. Chou CJ, Peng SY, Wu MH, Yang CC, Lin YS, Cheng WT, Wu SC, Lin YP (2014) Generation and characterization of a transgenic pig carrying a DsRed-monomer reporter gene. PLoS One 9:e106864.
13. Daniel K, Icha J, Horenburg C, Muller D, Norden C, Mansfeld J (2018) Conditional control of fluorescent protein degradation by an auxin-dependent nanobody. Nat Commun 9:3297.
14. DiBenedictis BT, Helfand AI, Baum MJ, Cherry JA (2014) A quantitative comparison of the efferent projections of the anterior and posterior subdivisions of the medial amygdala in female mice. Brain Res 1543:101-108.
15. Doudna JA, Charpentier E (2014) Genome editing. The new frontier of genome engineering with CRISPR-Cas9. Science 346:1258096.
16. Fridy PC, Li Y, Keegan S, Thompson MK, Nudelman I, Scheid JF, Oeffinger M, Nussenzweig MC, Fenyo D, Chait BT, Rout MP (2014) A robust pipeline for rapid production of versatile nanobody repertoires. Nat Methods 11:1253-1260.
17. Fujihara K, Miwa H, Kakizaki T, Kaneko R, Mikuni M, Tanahira C, Tamamaki N, Yanagawa Y (2015) Glutamate Decarboxylase 67 Deficiency in a Subset of GABAergic Neurons Induces Schizophrenia-Related Phenotypes. Neuropsychopharmacology 40:2475-2486.
18. Furuta T, Tomioka R, Taki K, Nakamura K, Tamamaki N, Kaneko T (2001) In vivo transduction of central neurons using recombinant Sindbis virus: Golgi-like labeling of dendrites and axons with membrane-targeted fluorescent proteins. J Histochem Cytochem 49:1497-1508.
19. Gerdes C, Waal N, Offner T, Fornasiero EF, Wender N, Verbarg H, Manzini I, Trenkwalder C, Mollenhauer B, Strohaker T, Zweckstetter M, Becker S, Rizzoli SO, Basmanav FB, Opazo F (2020) A

nanobody-based fluorescent reporter reveals human alpha-synuclein in the cell cytosol. Nat Commun 11:2729.

20. Gertsik N, Chiu D, Li YM (2014) Complex regulation of gamma-secretase: from obligatory to modulatory subunits. Front Aging Neurosci 6:342.
21. Gulati S, Jin H, Masuho I, Orban T, Cai Y, Pardon E, Martemyanov KA, Kiser PD, Stewart PL, Ford CP, Steyaert J, Palczewski K (2018) Targeting G protein-coupled receptor signaling at the G protein level with a selective nanobody inhibitor. Nat Commun 9:1996.
22. Hall MP, Unch J, Binkowski BF, Valley MP, Butler BL, Wood MG, Otto P, Zimmerman K, Vidugiris G, Machleidt T, Robers MB, Benink HA, Eggers CT, Slater MR, Meisenheimer PL, Klaubert DH, Fan F, Encell LP, Wood KV (2012) Engineered luciferase reporter from a deep sea shrimp utilizing a novel imidazopyrazinone substrate. ACS Chem Biol 7:1848-1857.
23. Heidenreich M, Zhang F (2016) Applications of CRISPR-Cas systems in neuroscience. Nat Rev Neurosci 17:36-44.
24. Helma J, Cardoso MC, Muyldermans S, Leonhardt H (2015) Nanobodies and recombinant binders in cell biology. J Cell Biol 209:633-644.
25. Hernandez VM, Hegeman DJ, Cui Q, Kelver DA, Fiske MP, Glajch KE, Pitt JE, Huang TY, Justice NJ, Chan CS (2015) Parvalbumin+ Neurons and Npas1+ Neurons Are Distinct Neuron Classes in the Mouse External Globus Pallidus. J Neurosci 35:11830-11847.
26. Htun H, Barsony J, Renyi I, Gould DL, Hager GL (1996) Visualization of glucocorticoid receptor translocation and intranuclear organization in living cells with a green fluorescent protein chimera. Proc Natl Acad Sci U S A 93:4845-4850.
27. Huang S, Chen J, Chen Q, Wang H, Yao Y, Chen J, Chen Z (2013) A second CRM1-dependent nuclear export signal in the influenza A virus NS2 protein contributes to the nuclear export of viral ribonucleoproteins. J Virol 87:767-778.
28. Imayoshi I, Isomura A, Harima Y, Kawaguchi K, Kori H, Miyachi H, Fujiwara T, Ishidate F, Kageyama R (2013) Oscillatory control of factors determining multipotency and fate in mouse neural progenitors. Science 342:1203-1208.
29. Inoue M, Takeuchi A, Horigane S, Ohkura M, Gengyo-Ando K, Fujii H, Kamijo S, Takemoto-Kimura S, Kano M, Nakai J, Kitamura K, Bito H (2015) Rational design of a high-affinity, fast, red calcium indicator R-CaMP2. Nat Methods 12:64-70.
30. Inutsuka A, Kimizuka N, Takanohashi N, Yakabu H, Onaka T (2020) Visualization of a blue light transmission area in living animals using light-induced nuclear translocation of fluorescent proteins. Biochem Biophys Res Commun 522:138-143.
31. Inutsuka A, Inui A, Tabuchi S, Tsunematsu T, Lazarus M, Yamanaka A (2014) Concurrent and robust regulation of feeding behaviors and metabolism by orexin neurons. Neuropharmacology 85:451-460.
32. Inutsuka A, Yamashita A, Chowdhury S, Nakai J, Ohkura M, Taguchi T, Yamanaka A (2016) The integrative role of orexin/hypocretin neurons in nociceptive perception and analgesic regulation. Sci Rep 6:29480.

33. Irannejad R, Tomshine JC, Tomshine JR, Chevalier M, Mahoney JP, Steyaert J, Rasmussen SG, Sunahara RK, El-Samad H, Huang B, von Zastrow M (2013) Conformational biosensors reveal GPCR signalling from endosomes. Nature 495:534-538.
34. Katoh A, Fujihara H, Ohbuchi T, Onaka T, Hashimoto T, Kawata M, Suzuki H, Ueta Y (2011) Highly visible expression of an oxytocin-monomeric red fluorescent protein 1 fusion gene in the hypothalamus and posterior pituitary of transgenic rats. Endocrinology 152:2768-2774.
35. Kawano F, Suzuki H, Furuya A, Sato M (2015) Engineered pairs of distinct photoswitches for optogenetic control of cellular proteins. Nat Commun 6:6256.
36. Kawano F, Okazaki R, Yazawa M, Sato M (2016) A photoactivatable Cre-loxP recombination system for optogenetic genome engineering. Nat Chem Biol 12:1059-1064.
37. Kirchhofer A, Helma J, Schmidthals K, Frauer C, Cui S, Karcher A, Pellis M, Muyldermans S, Casas-Delucchi CS, Cardoso MC, Leonhardt H, Hopfner KP, Rothbauer U (2010) Modulation of protein properties in living cells using nanobodies. Nat Struct Mol Biol 17:133-138.
38. Kopan R, Ilagan MX (2009) The canonical Notch signaling pathway: unfolding the activation mechanism. Cell 137:216-233.
39. Kredel S, Oswald F, Nienhaus K, Deuschle K, Rocker C, Wolff M, Heilker R, Nienhaus GU, Wiedenmann J (2009) mRuby, a bright monomeric red fluorescent protein for labeling of subcellular structures. PLoS One 4:e4391.
40. Liu Z et al. (2016) Autism-like behaviours and germline transmission in transgenic monkeys overexpressing MeCP2. Nature 530:98-102.
41. Lupien SJ, McEwen BS, Gunnar MR, Heim C (2009) Effects of stress throughout the lifespan on the brain, behaviour and cognition. Nat Rev Neurosci 10:434-445.
42. Mikuni S, Tamura M, Kinjo M (2007) Analysis of intranuclear binding process of glucocorticoid receptor using fluorescence correlation spectroscopy. FEBS Lett 581:389-393.
43. Nagai T, Ibata K, Park ES, Kubota M, Mikoshiba K, Miyawaki A (2002) A variant of yellow fluorescent protein with fast and efficient maturation for cell-biological applications. Nat Biotechnol 20:87-90.
44. Nasanbuyan N, Yoshida M, Takayanagi Y, Inutsuka A, Nishimori K, Yamanaka A, Onaka T (2018) Oxytocin-Oxytocin Receptor Systems Facilitate Social Defeat Posture in Male Mice. Endocrinology 159:763-775.
45. Niopek D, Wehler P, Roensch J, Eils R, Di Ventura B (2016) Optogenetic control of nuclear protein export. Nat Commun 7:10624.
46. Ran FA, Hsu PD, Wright J, Agarwala V, Scott DA, Zhang F (2013) Genome engineering using the CRISPR-Cas9 system. Nat Protoc 8:2281-2308.
47. Roesler R, Schwartsmann G (2012) Gastrin-releasing peptide receptors in the central nervous system: role in brain function and as a drug target. Front Endocrinol (Lausanne) 3:159.
48. Saederup N, Cardona AE, Croft K, Mizutani M, Cotleur AC, Tsou CL, Ransohoff RM, Charo IF (2010) Selective chemokine receptor usage by central nervous system myeloid cells in CCR2-red fluorescent

protein knock-in mice. PLoS One 5:e13693.

49. Sagoshi S, Maejima S, Morishita M, Takenawa S, Otubo A, Takanami K, Sakamoto T, Sakamoto H, Tsukahara S, Ogawa S (2020) Detection and Characterization of Estrogen Receptor Beta Expression in the Brain with Newly Developed Transgenic Mice. Neuroscience 438:182-197.
50. Sasaki E et al. (2009) Generation of transgenic non-human primates with germline transmission. Nature 459:523-527.
51. Shaner NC, Steinbach PA, Tsien RY (2005) A guide to choosing fluorescent proteins. Nat Methods 2:905-909.
52. Shaner NC, Campbell RE, Steinbach PA, Giepmans BN, Palmer AE, Tsien RY (2004) Improved monomeric red, orange and yellow fluorescent proteins derived from Discosoma sp. red fluorescent protein. Nat Biotechnol 22:1567-1572.
53. Shen Y, Lai T, Campbell RE (2015) Red fluorescent proteins (RFPs) and RFP-based biosensors for neuronal imaging applications. Neurophotonics 2:031203.
54. Stumpp MT, Binz HK, Amstutz P (2008) DARPins: a new generation of protein therapeutics. Drug Discov Today 13:695-701.
55. Subach FV, Patterson GH, Manley S, Gillette JM, Lippincott-Schwartz J, Verkhusha VV (2009) Photoactivatable mCherry for high-resolution two-color fluorescence microscopy. Nat Methods 6:153-159.
56. Suzuki S, Handa RJ (2005) Estrogen receptor-beta, but not estrogen receptor-alpha, is expressed in prolactin neurons of the female rat paraventricular and supraoptic nuclei: comparison with other neuropeptides. J Comp Neurol 484:28-42.
57. Takanami K, Uta D, Matsuda KI, Kawata M, Carstens E, Sakamoto T, Sakamoto H (2021) Estrogens influence female itch sensitivity via the spinal gastrin-releasing peptide receptor neurons. Proc Natl Acad Sci U S A 118.
58. Tang JC, Szikra T, Kozorovitskiy Y, Teixiera M, Sabatini BL, Roska B, Cepko CL (2013) A nanobody-based system using fluorescent proteins as scaffolds for cell-specific gene manipulation. Cell 154:928-939.
59. Tang JC, Drokhlyansky E, Etemad B, Rudolph S, Guo B, Wang S, Ellis EG, Li JZ, Cepko CL (2016) Detection and manipulation of live antigen-expressing cells using conditionally stable nanobodies. Elife 5.
60. Tang JC, Rudolph S, Dhande OS, Abraira VE, Choi S, Lapan SW, Drew IR, Drokhlyansky E, Huberman AD, Regehr WG, Cepko CL (2015) Cell type-specific manipulation with GFP-dependent Cre recombinase. Nat Neurosci 18:1334-1341.
61. Uenoyama Y, Nakamura S, Hayakawa Y, Ikegami K, Watanabe Y, Deura C, Minabe S, Tomikawa J, Goto T, Ieda N, Inoue N, Sanbo M, Tamura C, Hirabayashi M, Maeda KI, Tsukamura H (2015) Lack of pulse and surge modes and glutamatergic stimulation of luteinising hormone release in Kiss1 knockout rats. J Neuroendocrinol 27:187-197.

62. Wang LL, Serrano C, Zhong X, Ma S, Zou Y, Zhang CL (2021) Revisiting astrocyte to neuron conversion with lineage tracing in vivo. Cell 184:5465-5481 e5416.
63. Wilton EE, Opyr MP, Kailasam S, Kothe RF, Wieden HJ (2018) sdAb-DB: The Single Domain Antibody Database. ACS Synth Biol 7:2480-2484.
64. Yamagata M, Sanes JR (2018) Reporter-nanobody fusions (RANbodies) as versatile, small, sensitive immunohistochemical reagents. Proc Natl Acad Sci U S A 115:2126-2131.
65. Yao X, Liu Z, Wang X, Wang Y, Nie YH, Lai L, Sun R, Shi L, Sun Q, Yang H (2018) Generation of knock-in cynomolgus monkey via CRISPR/Cas9 editing. Cell Res 28:379-382.
66. Zhou XX, Chung HK, Lam AJ, Lin MZ (2012) Optical control of protein activity by fluorescent protein domains. Science 338:810-814.

Figures

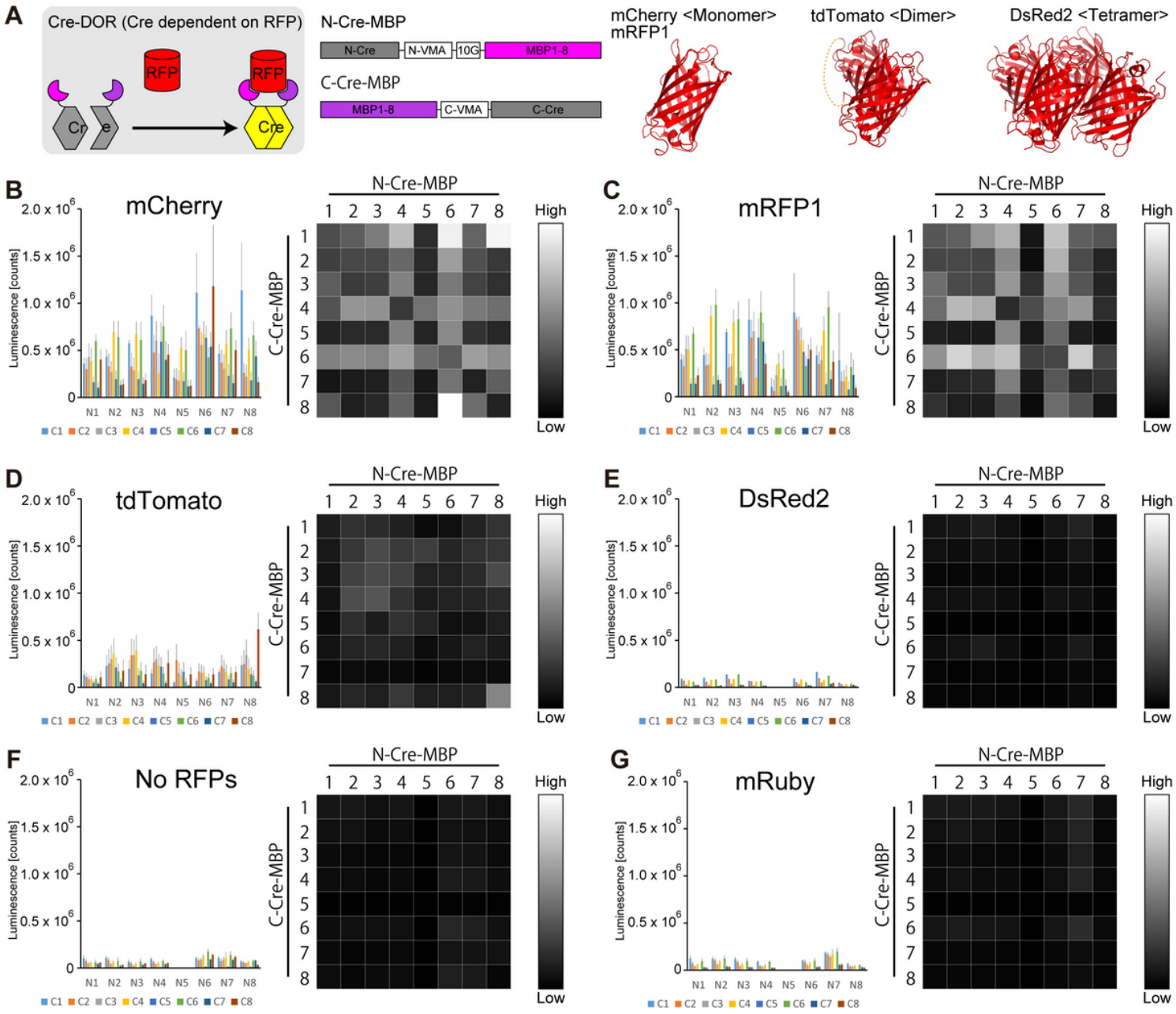

Figure 1

Luciferase assay screening of efficient MBP pairs for Cre-DOR.

A, Schematic presentation of the construct of Cre-DOR. N- or C-terminal split Cre recombinase is fused with mCherry-binding nanobody or DARPin. Binding of RFPs induces reunion of N-Cre and C-Cre into functional Cre recombinase. While mCherry and mRFP1 are monomeric, tdTomato is dimeric. ***B-G,*** Luciferase assay screening of functional pairs of MBPs for mCherry (**B**), mRFP1 (**C**), tdTomato (**D**), DsRed2 **(E)**, No RFPs **(F)** and mRuby **(G)**. Every intensity value was normalized by the maximum value and the normalized value is indicated as brightness of 256 levels of gray.

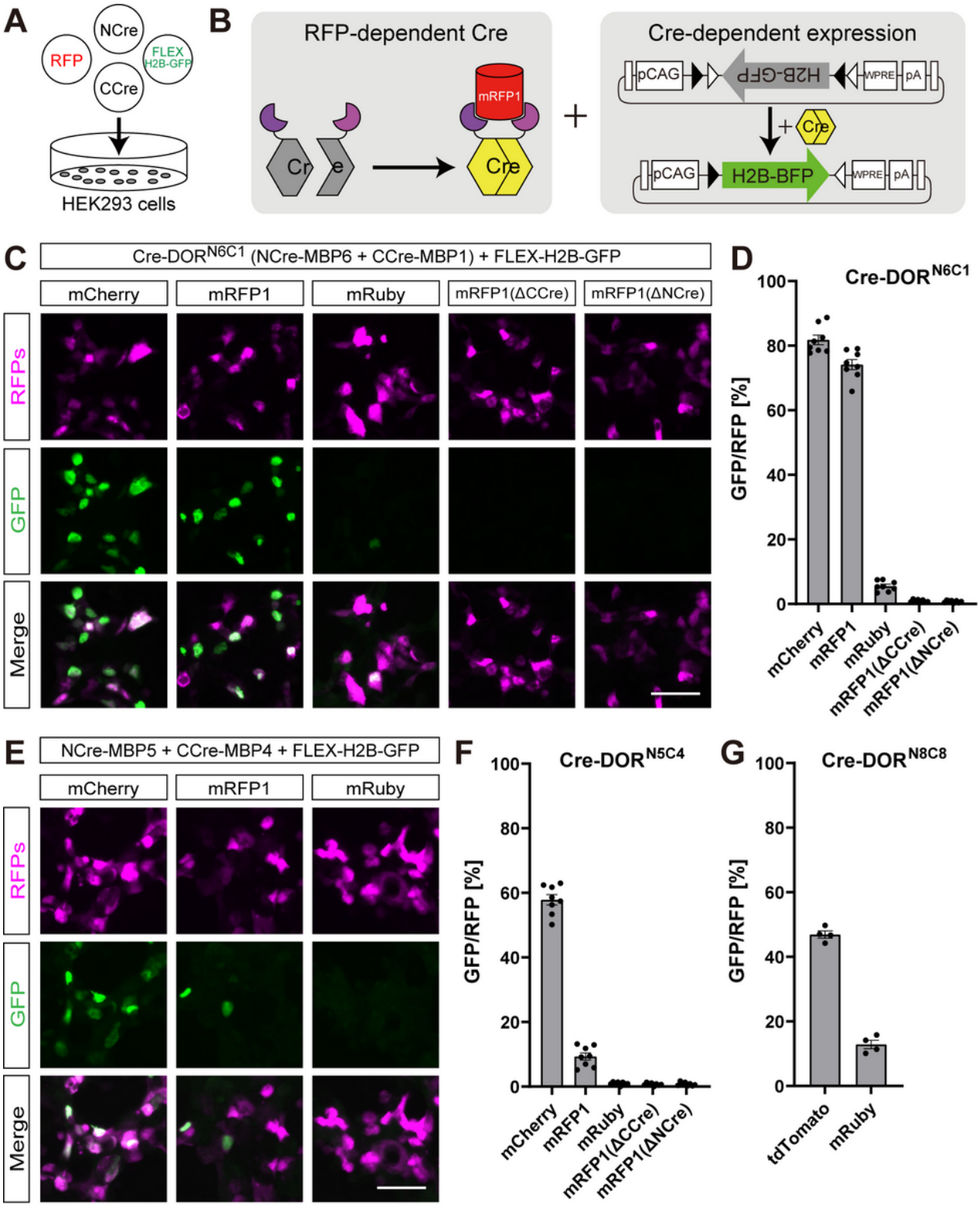

Figure 2

Functional assay of Cre-DOR in HEK293 cells.

A, Schematic illustration of Cre-DOR transfection in HEK293 cells. Four kinds of plasmids (NCre-MBP, CCre-MBP, FLEX-H2B-GFP, and target RFPs) were transfected in HEK293 cells to assess Cre-DOR recombination efficiency. ***B,*** Illustration of specific expression of H2B-GFP induced by Cre-DOR activated

by mRFP1. ***C,*** Fluorescent images of reporter H2B-GFP expression in transfected HEK293 cells to assess Cre-DOR (N-Cre-MBP6 and C-Cre-MBP1) efficiency for target RFPs. ***D,*** Quantification of cell counts in transfected HEK293 cells to assess Cre-DOR (N-Cre-MBP6 and C-Cre-MBP1) efficiency for all components of the system. ***E,*** Fluorescent images of reporter H2B-GFP expression in transfected HEK293 cells to assess Cre-DOR (N-Cre-MBP5 and C-Cre-MBP4) efficiency for target RFPs. ***F,*** Quantification of cell counts in transfected HEK293 cells to assess Cre-DOR (N-Cre-MBP5 and C-Cre-MBP4) efficiency for all components of the system. Data are means ± SEM (n = 8 or n = 4 in ***G***). Scale bar = 50 µm.

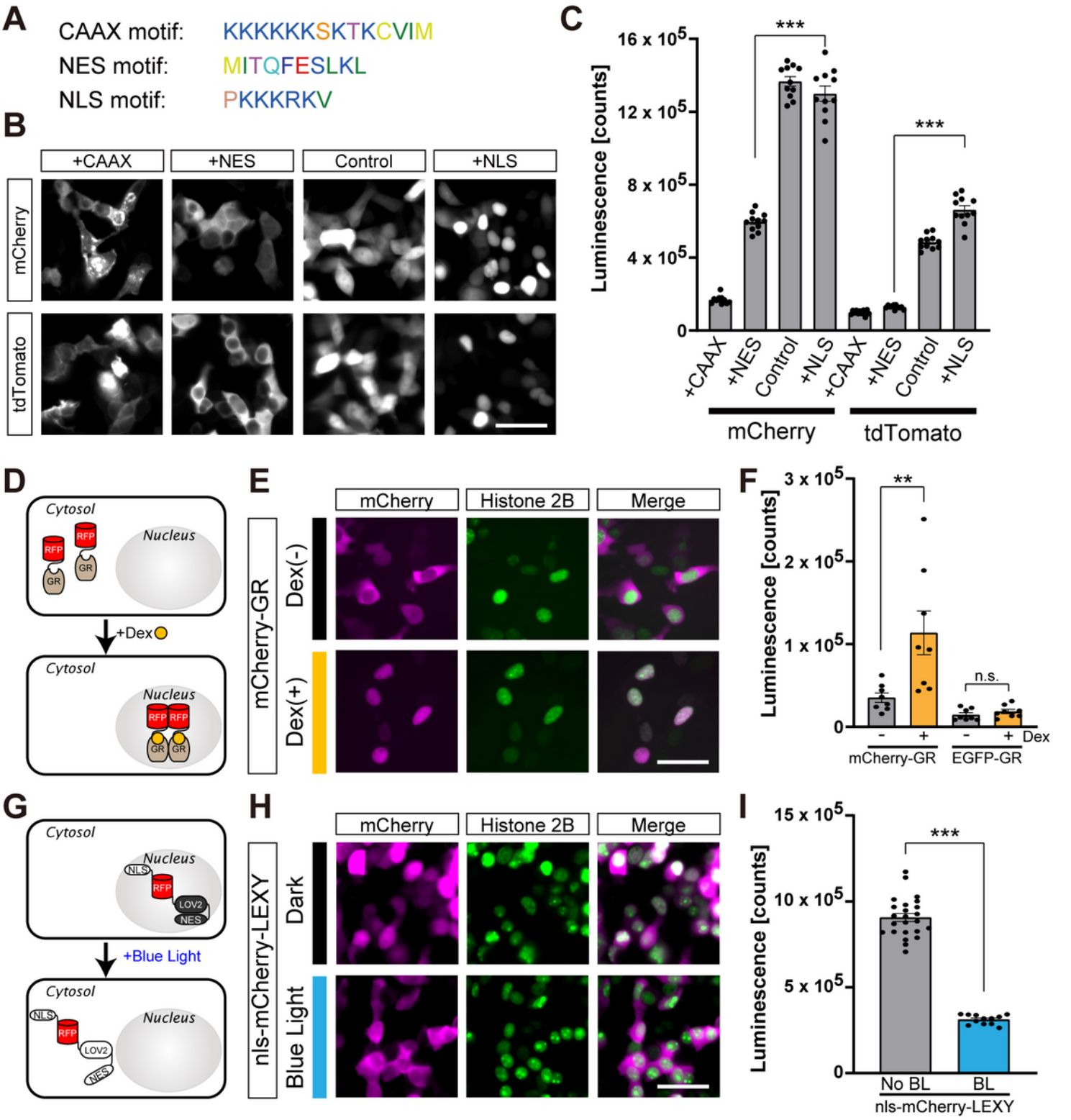

Figure 3

Cellular localization and recombinase activity of Cre-DOR.

A, Amino acid sequences of the CAAX motif (membrane localization signal), NES motif (nuclear export signal), and NLS motif (nuclear localization signal). ***B,*** Fluorescent images of mCherry or tdTomato with or without (Control) each localization motif. Scale bar = 50 μm. ***C,*** Luciferase assay of Cre-DOM or Cre-DOT with RFPs having different cellular localizations. Data are means ± SEM. Statistical analyses were performed by one-way ANOVA followed by Tukey's multiple comparison test (n = 11, *** $P < 0.001$). ***D,*** Schematic representation of ligand-induced translocation of RFPs from the cytosol to the nucleus. Dexamethasone (Dex) induces translocation of GRs upon its binding. ***E,*** Fluorescent images of mCherry-GR without or with Dex (1 μM, 1 hour). Scale bar = 50 μm. ***F,*** Luciferase assay of Cre-DOR^{N6C1} activity targeting mCherry-GR without or with Dex (1 μM, 24 hours). Data are means ± SEM. Statistical analyses were performed by one-way ANOVA followed by Tukey's multiple comparison test (n = 8, ** $P < 0.01$). ***G,*** Schematic representation of light-induced translocation of RFPs from the nucleus to the cytosol. The LEXY domain consists of a modified AsLOV2 domain with NES. Blue light induces exposure of the NES and results in translocation of RFPs. ***H,*** Fluorescent images of nls-mCherry-LEXY with or without blue light illumination (465 nm, 3.7 W/m^2). Scale bar = 50 μm. ***I,*** Luciferase assay of Cre-DOM activity targeting nls-mCherry-LEXY without or with blue light illumination (n = 24, 12). Data are means ± SEM. Statistical analyses were performed by Student's t-test (*** $P < 0.001$). In **Figure 3E and 3H**, nuclei are visualized by fluorescence from H2B-BFP that was co-transfected with mCherry-GR or nls-mCherry-LEXY.

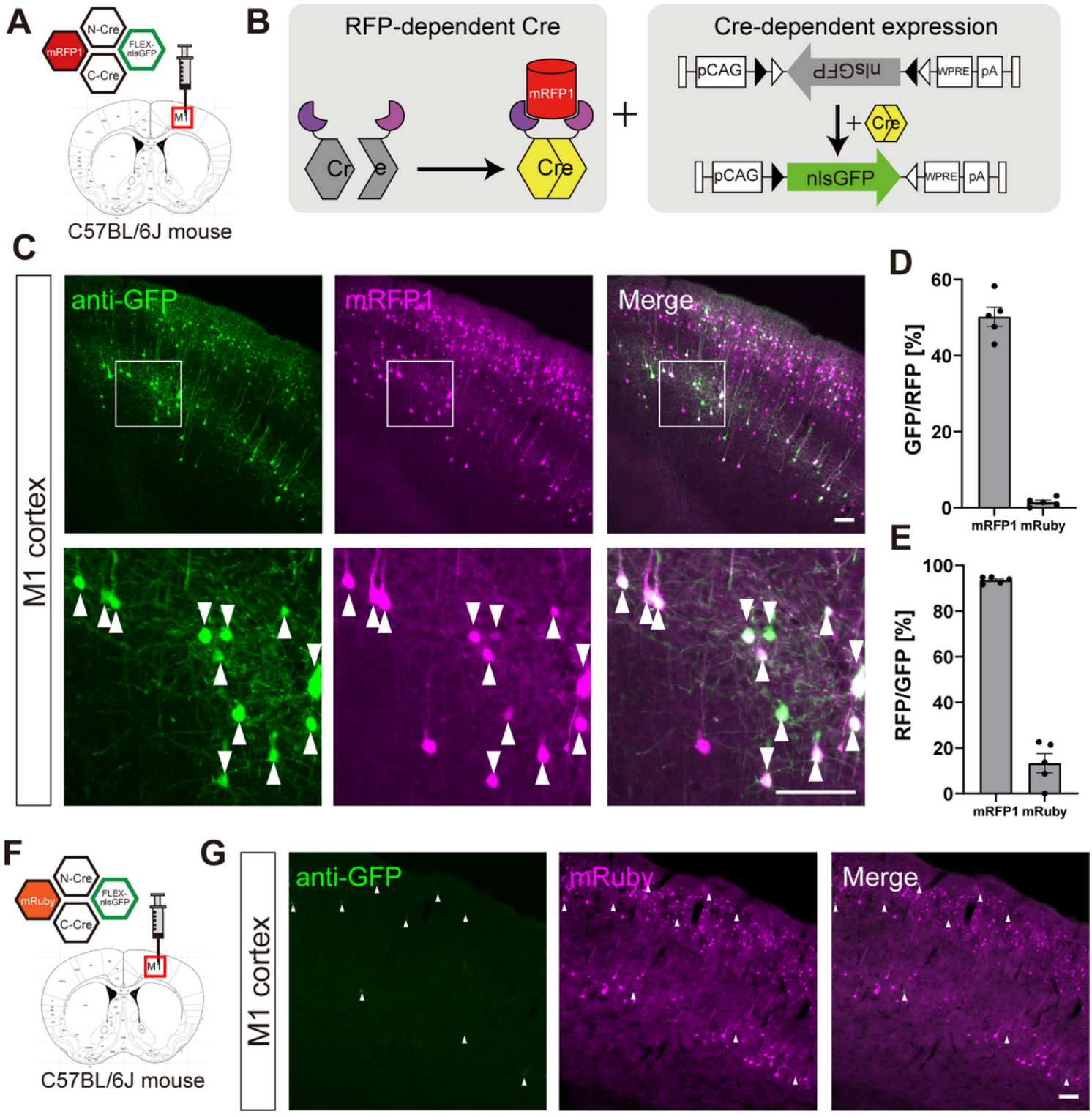

Figure 4

Functional assay of Cre-DOR^{N6C1} *in vivo*.

A, Injection schema of the Cre-DOR^{N6C1} test with mRFP1 in wild-type mice. Four kinds of virus (NCre-MBP6, CCre-MBP1, FLEX-nlsGFP, and mRFP1) were injected in the M1 cortex at the same time. ***B,*** Schematic representation of specific expression of nlsGFP induced by Cre-DOR activated by mRFP1. ***C,*** Fluorescent images of the M1 cortex. Scale bar = 100 μm. ***D,*** Quantification of cell counts to assess the

efficiency of Cre-DOR^{N6C1} (n = 5 each). ***E,*** Quantification of cell counts to assess the fidelity of Cre-DOR^{N6C1} (n = 5 each). ***F,*** Injection schema of the Cre-DOR^{N6C1} test with mRuby in wild-type mice. ***G,*** Fluorescent images of the M1 cortex in which the four viruses were injected. Scale bar = 100 μm. Data are means ± SEM.

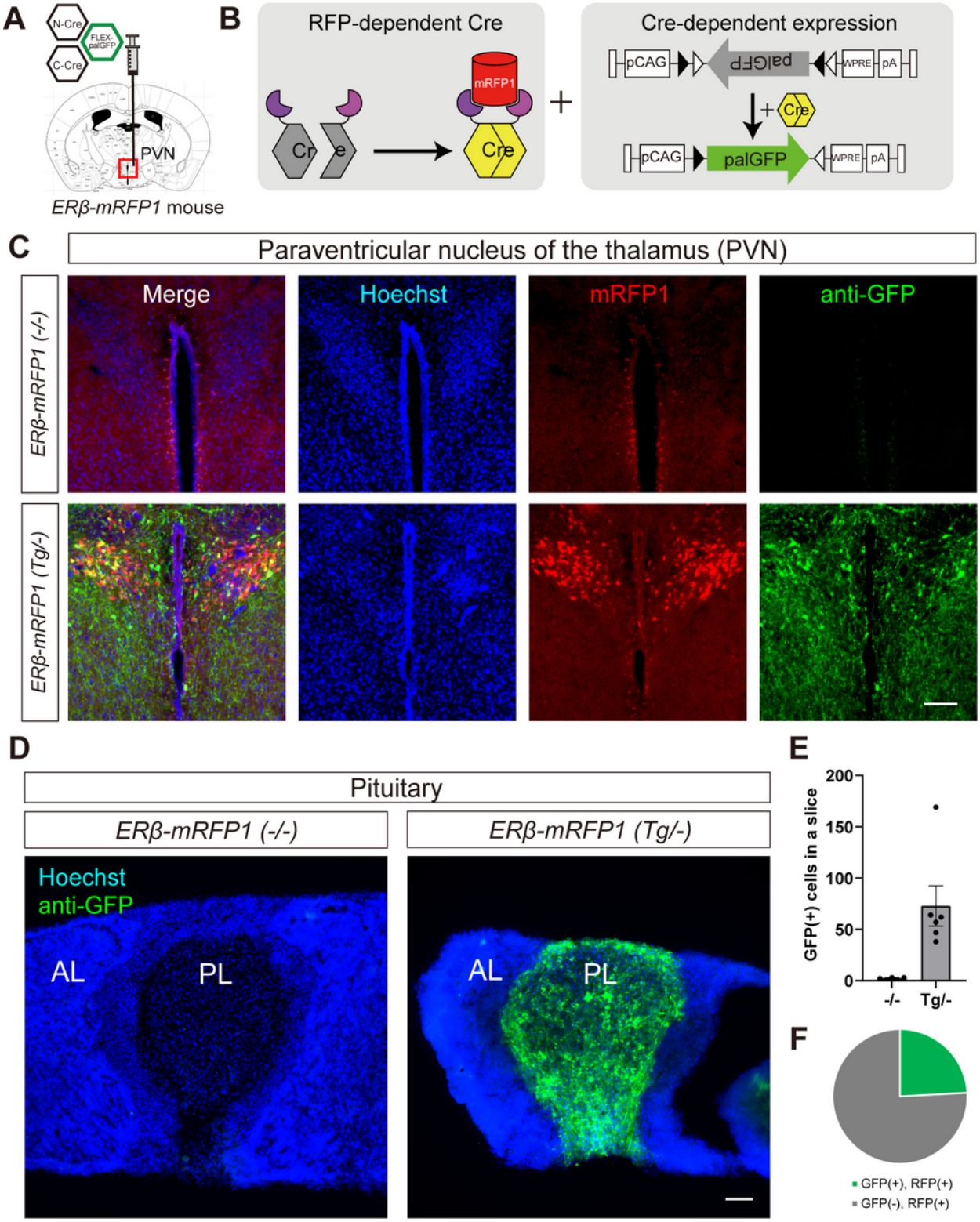

Figure 5

Anterograde tracing using Cre-DOR in *Esr2*-mRFP1 transgenic mice.

A, Stereotaxic injection schema of Cre-DOR^{N6C1} in *Esr2*-mRFP1 transgenic mice. Three kinds of virus (NCre-MBP6, CCre-MBP1, FLEX-palGFP) were injected in the paraventricular nucleus (PVN). ***B,*** Schematic representation of specific expression of palGFP induced by Cre-DOR activated by mRFP1.***C,*** Immunofluorescent images of the PVN of injected mice. Scale bar = 100 μm. ***D,*** Representative images of axonal projection from palGFP-expressing neurons in the PVN of *Esr2*-mRFP1 transgenic mice. AL: anterior lobe, PL: posterior lobe. Scale bar = 100 μm.***E,*** Quantification of mRFP1-induced expression of palGFP in WT and Tg *Esr2*-mRFP1 *mice*. ***F,*** Cell counting results showing the average percentage of palGFP-positive cells in the PVN of the Cre-DOR virus-injected *Esr2*-mRFP1 transgenic mice.

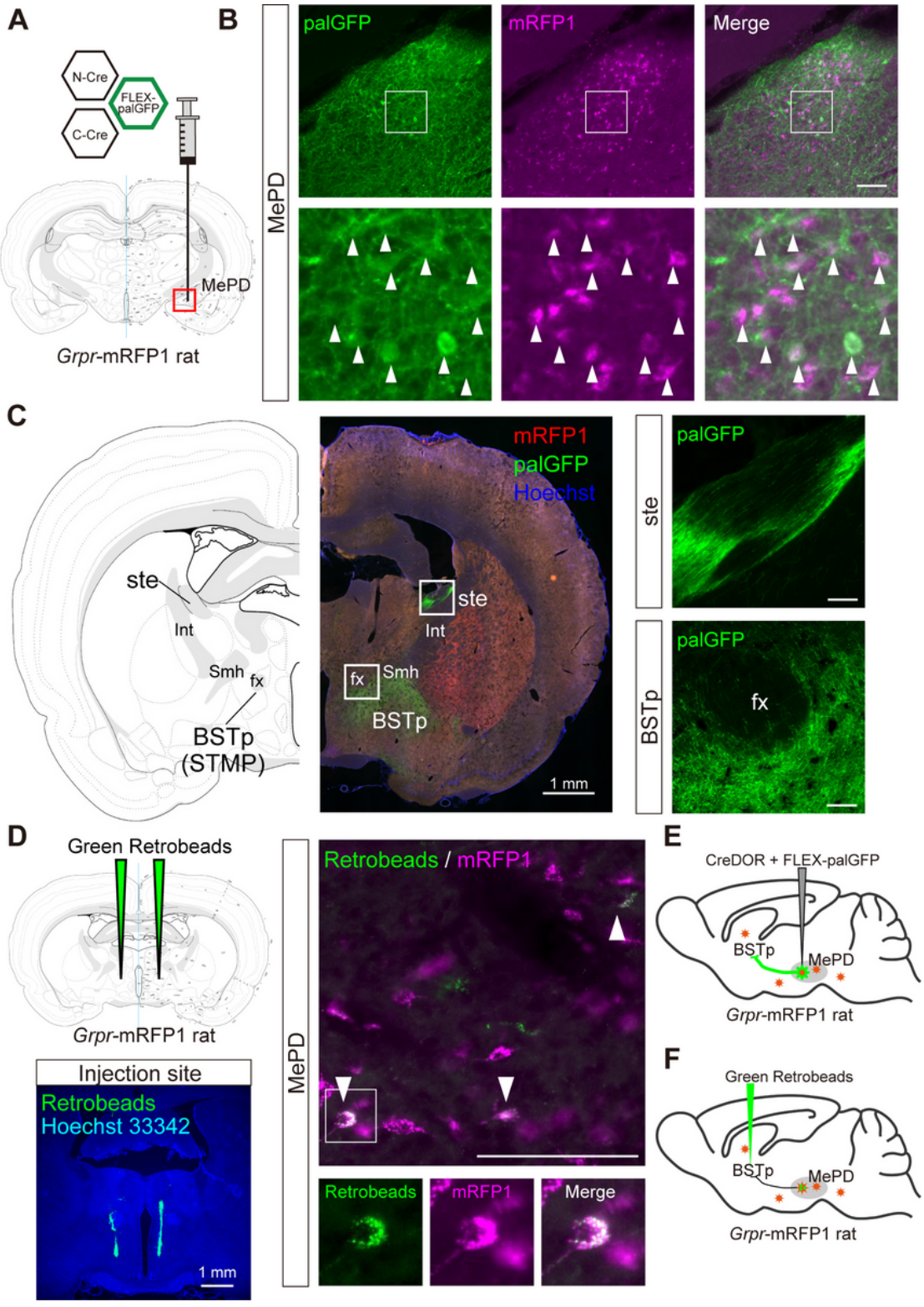

Figure 6

Anterograde tracing using Cre-DOR in transgenic mRFP1-expressing rats.

A, Stereotaxic injection schema of Cre-DOR^{N6C1} in *Grpr*-mRFP1 transgenic rats. Three kinds of virus (NCre-MBP6, CCre-MBP1, FLEX-palGFP) were injected in the medial amygdala. ***B,*** Immunofluorescent images of the MePD of injected rats. Scale bar = 100 μm. ***C,*** A representative image of axonal projection

from palGFP-expressing neurons in the MePD of a *Grpr*-mRFP1 transgenic rat. Scale bar = 100 μm or 1 mm. ***D,*** Injection schema of green retrobeads in a *Grpr*-mRFP1 rat. Scale bar = 100 μm or 1 mm. ***E,*** Illustration of anterograde tracing using Cre-DOR in *Grpr*-mRFP1 rats. ***F,*** Illustration of retrograde tracing using green retrobeads in *Grpr*-mRFP1 rats.

Supplementary Files

This is a list of supplementary files associated with this preprint. Click to download.

- SupplementalFigure1.jpg
- SupplementalFigure2.jpg